Hindawi
Advances in Polymer Technology
Volume 2022, Article ID 9772946, 9 pages
https://doi.org/10.1155/2022/9772946

WILEY | Hindawi

Research Article

Study on the Stress–Strain Relationships and Deterioration Modes of HTPB Propellant with Prefabricated Cracks

Bo Gao and Zhuo Li

College of Science, Inner Mongolia University of Technology, Hohhot 010051, China

Correspondence should be addressed to Zhuo Li; 704028389@qq.com

Received 16 May 2022; Revised 30 June 2022; Accepted 15 July 2022; Published 10 August 2022

Academic Editor: Kinga Pielichowska

Penetrating cracks with different crack angles were prefabricated in viscoelastic hydroxyl-terminated polybutadiene propellant specimens. Microphotography was performed while tensile tests were conducted on a universal testing machine at tensile rates of 2 mm/min, 10 mm/min, and 500 mm/min. Specimen measurements were obtained by digital image correlation (DIC). The strain fields on the surfaces and around the cracks were studied, and the crack propagation trends for precracked specimens with angles of 0°, 45°, and 75° with respect to the horizontal plane were investigated. Stress–strain curves, tensile microscopic images (50x magnification), and fracture microscopic images (100x magnification) were obtained for different prefabricated crack angles and different stretching rates. It was observed that under low-rate stretching, the propellant crack growth exhibited three stages: a linear stage, a yield stage, and a failure stage. However, the crack propagation in the propellant under high-speed stretching had no yield stage. When there were no prefabricated cracks, a greater tensile rate led to a greater ultimate strain. The maximum strains at the crack tips measured by DIC decreased from group C1 to groups C2, C3, and S. The specimens corresponding to different crack inclination angles are pulled off. It was seen that the closer a crack was to positive breaking, the straighter was the edge notch of the specimen.

1. Introduction

The solid rocket motor is the main power source in a rocket, and hydroxyl-terminated polybutadiene (HTPB) propellant is one of the primary fuels used in solid rocket motors. While using and storing propellants, as the storage time increases, the mechanical properties of the propellants deteriorate, and the structures are prone to cracking and other types of damage. In serious cases, the cracks may expand to form unstable fractures. The mechanical properties of propellants experiencing external loads have been studied because they significantly impact overall engine stability.

To study the damage evolution trends of composite solid propellants, Feng et al. [1] built a mesostructure model for HTPB propellant based on the molecular dynamics particle-filling algorithm and simulated AP(ammonium perchlorate) particles and HTPB using bilinear and custom exponential damage cohesion models. The process of damage initiation, development, aggregation, and macroscopic crack failure was investigated at the substrate bonding interface. Gu et al. [2] chose the microcrack density as the damage variable on the mesoscopic scale and developed a damage constitutive model for composite solid propellants. Fan et al. [3] conducted tensile tests on silicone rubber at different loading rates and observed the fracture of the tensile specimens using a scanning electron microscope (SEM). The fracture behavior of the silicone rubber was studied at various loading rates less than 500 mm/min. Li et al. [4] conducted a multirate uniaxial tensile test with NEPE propellant, observed the tensile fracture using an SEM, and studied the mechanical properties and damage process of the NEPE propellant at different confining pressure conditions. Liu et al. [5] performed a uniaxial tensile mechanical properties test for a modified double-base propellant at different rates, observed the morphology of the tensile section using an SEM, and analyzed the effect of the tensile rate on the mechanical properties and section of the propellant. The effects on the morphology and the failure modes at

different stretching rates were investigated. To study the effect of aging on the fracture properties of HTPB propellant, Chang et al. [6] conducted a high-temperature accelerated aging test using HTPB propellant, measured the fracture toughness of the propellant with type I cracks at different aging times and aging temperatures, and used an SEM to observe the microscopic morphology of a propellant section. Zhu et al. [7] studied the quasistatic mechanical properties of an HTPE/AP/Al/RDX propellant within a wide temperature range and obtained the temperature of the propellant between −50°C and 70°C. The stress–strain curves at five strain rates were used to analyze the damage and failure modes of the propellant using the cross-sectional topography method. Seyidoglu and Bohn [8] analyzed the effects of four different isocyanates and four different plasticizers on HTPB-based elastomers by quantitatively analyzing the loss factor shape, the tensile strength, and the deformation frequency shift. Geng et al. [9] used the viscoelastic finite element method to reflect the deformation of the crack tip with a sharp angle, an ellipse, and a circular crack tip. The maximum circumferential stress criterion and the maximum energy release rate criterion were used as standards for judging the crack propagation direction according to the J-integral. The initial propagation directions of cracks with different inclination angles could then be calculated. Gao et al. [10] employed the high-speed camera digital image correlation (DIC) method to study the displacement and strain fields at the crack tip region of a compact tensile (CT) specimen in a resonant fatigue crack growth test under a high-frequency sinusoidal alternating load during the steady-state crack growth stage. The relationship between the strain amplitude at the crack tip and the number of fatigue cycles when the fatigue crack was not propagating and the variation trends of the displacement and strain fields in the crack tip region when the fatigue crack grew to different lengths were both studied. Wang et al. [11] prefabricated HTPB propellant specimens with single-side notches and used an in situ digital imaging video recording system to obtain the crack propagation speed. It was found that the fracture characteristics were significantly rate-dependent, and that the J-integral changed significantly for different stretching rates. The use of the J-integral to evaluate the fracture properties of propellants was proposed. Jarocki et al. [12] used noncontact two-dimensional digital images to measure the solid response and temperature of HTPB propellant at different strain rates. Hamidpour et al. [13] used the DIC method to measure the fracture behavior of linear viscoelastic materials, using this method to verify his proposed meshless method of analyzing the fracture of viscoelastic materials. Xu et al. [14] used the Weibull distribution function to describe the mechanical behavior of damage evolution and developed a new nonlinear viscoelastic damage constitutive model. The accuracy of the model was verified using relaxation test and uniaxial tensile test results for the NEPE propellant. To further study the fracture characteristics of solid propellants, Han et al. [15] performed a crack propagation simulation. The calculation results showed that the fracture response had better performance when using an external cohesive zone model (CZM) than when using a predefined intrinsic CZM since the external CZM provided a more accurate fracture response to crack paths. Li et al. [16] explored the effect of crack angle on mechanical properties through stress–strain curves, studying the damage evolution trends of sandstone. Le et al. [17] performed a numerical simulation using the K-distribution based on the M-integral and the crack propagation process. The study used the maximum tensile stress criterion for brittle materials, and the trend observed was consistent with the law of primary crack propagation. Liu and Smith [18] measured the strain fields near the central crack tips in granular composites, studied the effect of the applied strain level on the strain field and the local damage, and investigated the fracture process near the crack tip. Long et al. [19] used the linear viscoelastic model to conduct a dynamic crack tip field simulation study of the grain ignition transient. The risk of crack initiation was successfully demonstrated. Gao and Zhang [20] used theoretical and experimental research methods to investigate crack and debonding propagation. They studied the crack initiation criteria, the factors affecting propagation, and the fracture properties of propellant materials. To obtain the crack propagation characteristics of HTPB propellant from a mesoscopic perspective and analyze the mesoscopic failure crack mechanisms, Wang et al. [21] observed the crack tip damage and propagation processes during a bending test, obtaining the crack growth and deformation morphologies at different deformation stages. The DIC method was used to analyze the picture sequence, and the deformation field at the propellant crack tip was obtained. Yang et al. [22] studied the mesodamage behavior of composite solid HTPB, NEPE, and GAP propellants using in situ tensile SEM experiments, digital image processing technology, and the fractal dimension theory to combine research methods both qualitatively and quantitatively. The generation and evolution of microcracks in the propellants were analyzed during the tensile process. To obtain the deformation field and J-integral measurements of a composite crack tip, Wang et al. [23] conducted a tensile observation test using a prefabricated HTPB propellant specimen with a center-penetrating composite crack. A deformation picture sequence of the composite crack specimen was obtained. The displacement and strain fields were also obtained for the specimen surface using the DIC method, and the J-integral of the composite crack tip was calculated using the J-integral theory and the deformation field obtained from the DIC method.

Based on the existing research, this study combined DIC technology and microscopic imaging technology to investigate a variety of prefabricated cracks in HTPB propellant specimens and conduct uniaxial tensile tests on the specimens. Overall, high-definition microscopic images of the specimens and high-definition images of the fracture surfaces of the specimens were used to study the deterioration of precracked HTPB propellant.

2. Prefabricated Crack Tensile Tests

2.1. Specimens. The tensile test specimens were HTPB specimens, and each had a central through-type crack. Figure 1

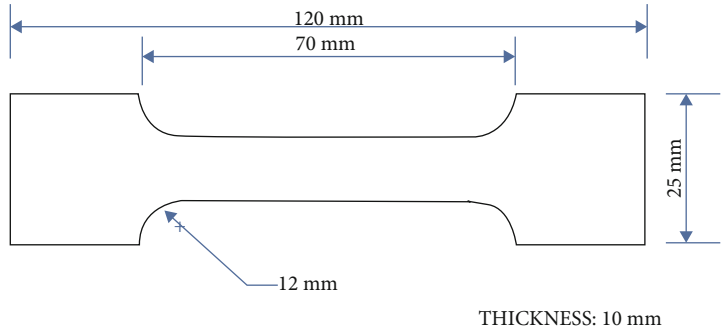

Figure 1: Size of the specimens.

shows the size of each specimen. The length was 120 mm, the width was 25 mm, the length of the observed area was 70 mm, the width of the observed area was 10 mm, and the thickness was 10 mm. A penetrating crack with a length of 2 mm was prefabricated in the middle of each specimen, and its width was not measured. The crack fabrication tool constructed in situ and the universal testing machine fixture are shown in Figure 2.

The production of the test specimens followed the "Ministry of Aerospace Industry of the People's Republic of China Standard QJ924-85" [24]. Figure 3 shows an example specimen after the crack was fabricated.

2.2. Equipment. The high-intensity microscope camera used in the tests was an Osmicro AO-HD228, a model which can achieve magnifications of 45x–400x and take pictures, as shown in Figure 2. The tests used a WDW-10 universal testing machine with a maximum testing force of 0.5 kN, as shown in Figure 2. The full-field strain measurement equipment used in the tests was the correlated SOLUTION VIC-3D System.

2.3. Experimental Process. The temperature of the test specimens was 20°C. The prepared precracked propellant specimens were installed on the universal testing machine, and the set rates were 2 mm/min, 10 mm/min, and 500 mm/min. The microscope camera and the DIC were installed synchronously, and these devices began and ended the experiments at the same time. Three to six sets of test specimens were tested for each set of working conditions, and the average of three sets of consistent test results was taken as the final test result. Stress–strain data, microscopic videos, and full-field strain data were obtained separately. Groups C1, C2, and C3 correspond to prefabricated cracks with horizontal angles of 0°, 45°, and 75°, respectively. Group S corresponds to a group without prefabricated cracks. A group name is marked with 2, 10, or 500 in parentheses according to its tensile rate; for example, a 2 mm/min tensile rate in the 0° crack group is labeled C1(2). The cracks damaged by normal stresses are type I cracks, and the cracks damaged by shear stresses are type II cracks. In this study, group C1 had typical type I cracks, and groups C2 and C3 had typical types I and II mixed cracks.

3. Analysis of the HTPB Propellant Uniaxial Tensile Test Results

3.1. Uniaxial Tensile Stress–Strain Results for the HTPB Propellant. Figure 4 shows that at tensile rates of 2 mm/min and 10 mm/min, the stress–strain curves exhibited typical three-stage characteristics. These stages included a linearly increasing trend at the initial stretching stage, a yield stage during which dehumidification occurred, and a rupture failure tearing stage. At a tensile rate of 500 mm/min, the specimens broke suddenly at the maximum strain point, and there was no obvious yield stage. Fracture failure occurred directly at the maximum strain point.

At a tensile rate of 2 mm/min, the maximum failure strain of the specimens without prefabricated cracks was the largest, approximately 0.62. In the prefabricated crack groups, the maximum failure strain for group C3 (75°) was the next largest, and the maximum failure strains for groups C1 and C2 were very small. The maximum failure strains for groups C3, C2, and C1 were 0.41, 0.33, and 0.32, respectively. For the tensile rate of 2 mm/min, the differences between the prefabricated 0° and 45° cracks had little effect on the extreme stresses and strains of failure.

At a tensile rate of 10 mm/min, similarly, the maximum failure strain of the specimen without precracking was larger than the others, with a maximum failure strain of 0.61. In the precracked groups, the maximum failure strain of group C3 (75°) was the largest, with a maximum failure strain of 0.38, followed by groups C1 and C2, with maximum failure strains of 0.36 and 0.32, respectively. However, the maximum failure strains of the three precracked groups were only slightly different. The maximum failure strains of these parts were nearly the same.

At a tensile rate of 500 mm/min, the maximum failure strain of the specimen without prefabricated cracks was the largest, with a maximum failure strain of 0.68. The maximum failure strains of the three groups with prefabricated cracks were relatively similar. The maximum failure strains of groups C1, C2, and C3 were 0.35, 0.37, and 0.42, respectively.

At the tensile rates of 2 mm/min, 10 mm/min, and 500 mm/min, the maximum failure strains of the specimens without precracking were significantly higher than the maximum failure strains of the precracked specimens. This result

(a) Universal testing machine

(b) High-intensity microscope camera

(c) DIC

Figure 2: Testing equipment.

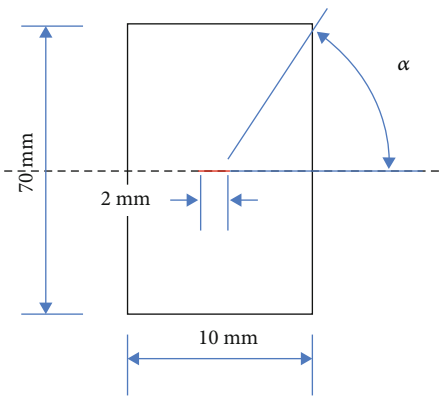

(a) Crack location

(b) Prefabricated cracked specimen

Figure 3: Prefabricated crack.

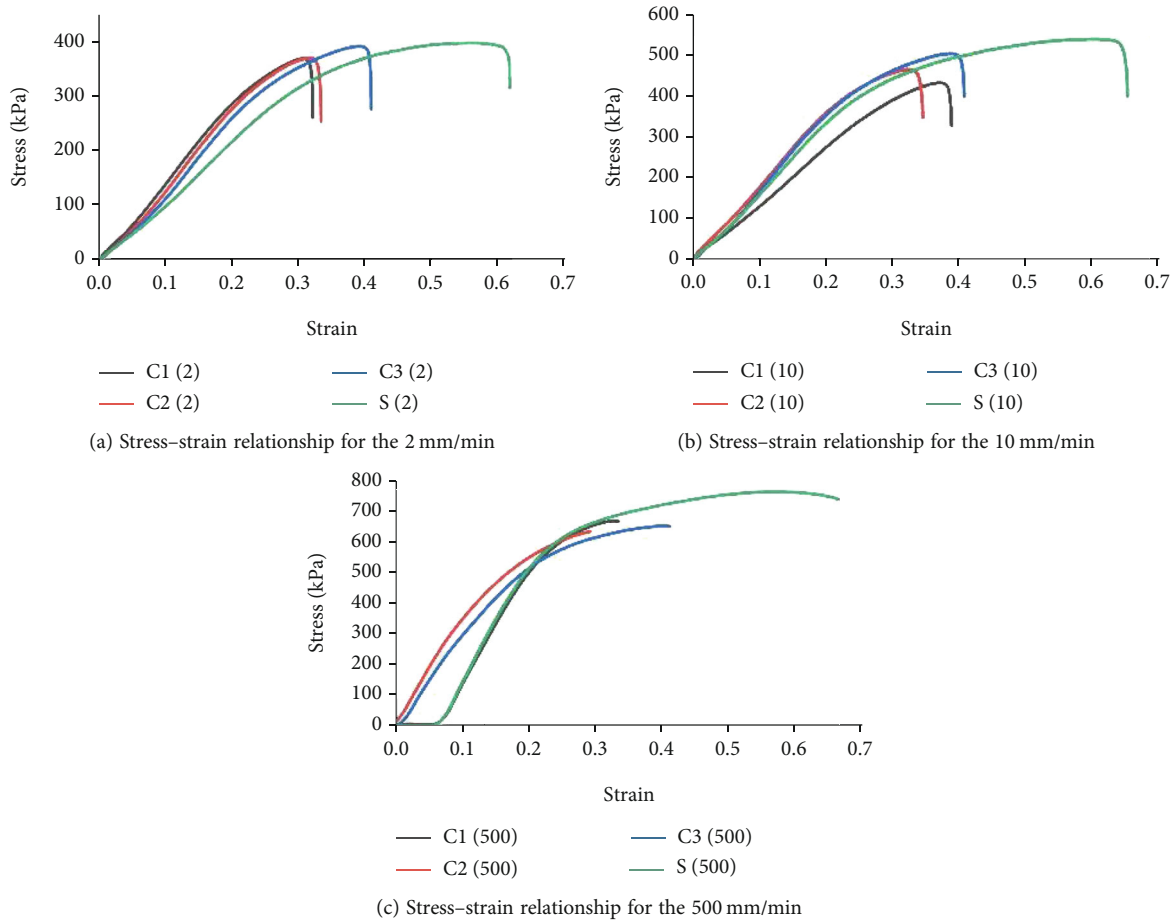

(a) Stress–strain relationship for the 2 mm/min

(b) Stress–strain relationship for the 10 mm/min

(c) Stress–strain relationship for the 500 mm/min

Figure 4: Stress–strain relationships corresponding to various strain rates.

demonstrates that the cracks were very important to the damage of the HTPB propellant shown in Figure 5. For the prefabricated crack groups, no matter which loading rate was used, the specimens with 75° prefabricated cracks were less likely to be damaged, and the ultimate failure strains of the other two groups were similar. The failure strains were similar but still slightly different. Under high-rate stretching, the failure strain differences for the three types of prefabricated cracks were very small. Therefore, the tensile rate significantly influenced the failure behavior of the precracked specimens.

3.2. HTPB Propellant Uniaxial Tensile Microphotography (MP) Analysis. During the uniaxial tensile tests, a microscope camera with 50x magnification was used to record the changes in the specimens throughout the entire process. The specimens were elongated in the loading direction under the three tensile rates, and the colors of the specimens did not change significantly. The specimens further deformed with the passage of the specimens, and the effective test sections began to show obvious AP particle precipitation. With further loading, the "dehumidification" effect was more pronounced; at this point, it was considered that the load on the propellant had reached its critical value. The particle–matrix interface inside the propellant had debonded and failed, and the matrix was left to bear the load alone. As the displacement load further increased, the matrix material continuously elongated, and the propellant eventually ruptured due to tearing.

For the C1 (0° crack) group, at tensile rates of 2 mm/min and 10 mm/min, crack propagation began at the edge and surrounded the entire crack from the periphery, and relatively obvious dehumidification phenomena occurred until the end of the test, and the matrix was torn and damaged. However, when the tensile rate was 500 mm/min, cracks began on all four sides at the same time, there were many microcracks, and there were no obvious dehumidification phenomena. Finally, this matrix also tore suddenly, failing. The cracks caused by the three rates were all typical type I cracks, as shown in Figure 5.

For the C2 (45° crack) group, the crack propagation showed an "hourglass-type" pattern at all three rates. Microcracks were generated at the tip of the crack, which continued to expand to form a larger "hourglass" until failure. There were obvious dehumidification phenomena for the 2 mm/min and 10 mm/min rates, but there was no obvious dehumidification at 500 mm/min, and brittle fracture occurred that led directly to failure. The C2 (45° crack) group exhibited typical types I and II composite cracks, as shown in Figure 6.

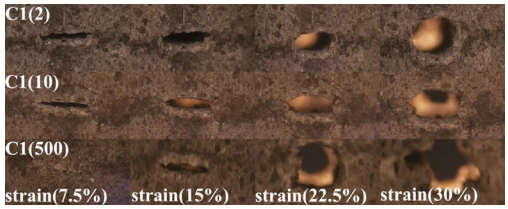

Figure 5: Microphotography (MP) results for group C1 (0° crack).

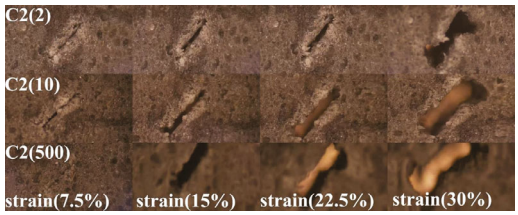

Figure 6: Microphotography (MP) results for group C2 (45° crack).

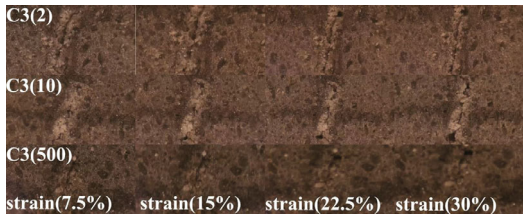

Figure 7: Microphotography (MP) results for group C3 (75° crack).

For the C3 (75° crack) group, as the strain increased, the crack area gradually became obvious, and there were microcracks at the crack tip, accompanied by a small amount of dehumidification. For all three rates, even at 30% strain, the crack was not especially obvious, indicating that the damage resistance of the 75° crack was still very good. The C3 (75° crack) group had types I and II composite cracks, as shown in Figure 7.

The compound cracks in groups C2 and C3 propagated along "zigzag" paths, and the angles between the "zigzags" decreased as the cracks expanded forward. The cracks exhibited transverse cracks after a certain number of "zigzag" bending and expansion changing trends. During the tests, regardless of the crack inclination angle in a specimen at the beginning of a test, after the crack began to expand, there was a transition to transverse cracking.

The specimens without prefabricated cracks did not change significantly with the different tensile rates, but it was observed that the pores in the matrix were stretched larger, and there was a small amount of dehumidification. There was no apparent failure within 30% strain, as shown in Figure 8.

From the maximum strain measured with the DIC method, the C1 (0°) and C2 (45°) groups exhibited relatively similar strain trends; fracture occurred at a small limit strain, and the maximum strain values reached 30%. The differences between group C3 (75°) and the first two groups were large, but the differences with respect to the group without

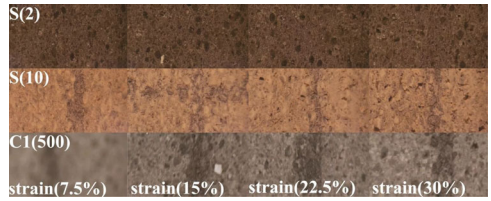

Figure 8: Microphotography (MP) results for group S (without precracking).

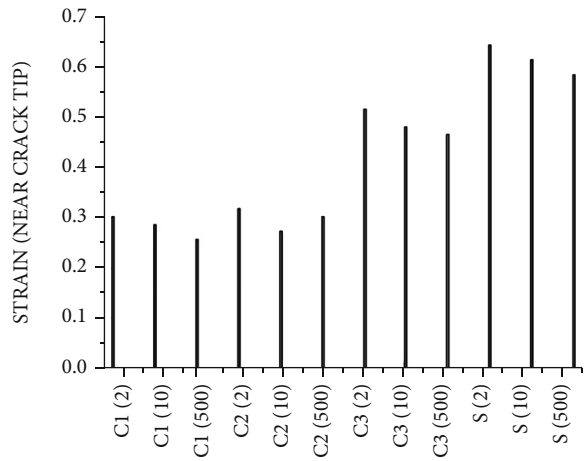

Figure 9: Maximum strain at the crack tip.

precracking were very small. The maximum strain values for the C3 and S groups exceeded 60%. The 75° crack did not affect the tensile failure of the propellant. The effects of the 0° and 45° cracks were large. In the C1, C2, C3, and S groups, the tensile rate significantly influenced the ultimate strain, and the ultimate failure strain gradually decreased from the 2 mm/min rate to the 10 mm/min and 500 mm/min rates. These decreases were due to the increase in the tensile rate and an increase in the proportion of brittle fracture failure, as is shown in Figure 9.

3.3. Overall Shapes of the HTPB Propellant Specimens after Uniaxial Tensile Failure. The fractures of the C1 (0°) specimens became increasingly smoother as the tensile rate increased, and this smoothness was particularly good. The C2 (45°) and C3 (75°) specimens showed inverse "Z"-shaped cracks at the three rates, and they gradually became flatter as the tensile rate increased. The fracture positions of the cracks were random regardless of the tensile rate; some were in the middle position and some were in the neck. This result also aligned with expectations, as is shown in Figure 10.

3.4. Micrograph Analysis of the Uniaxial Tensile Fracture of the HTPB Propellant (100x Magnification). The matrix, particles, and holes of the HTPB propellant surfaces could be seen by microscopic image observations. It was necessary to obtain key information, such as the particle shape and the particle–matrix interface bonding state, inside the propellant. This was done by observing the specimen

Figure 10: Overall shapes of the specimens after fracture.

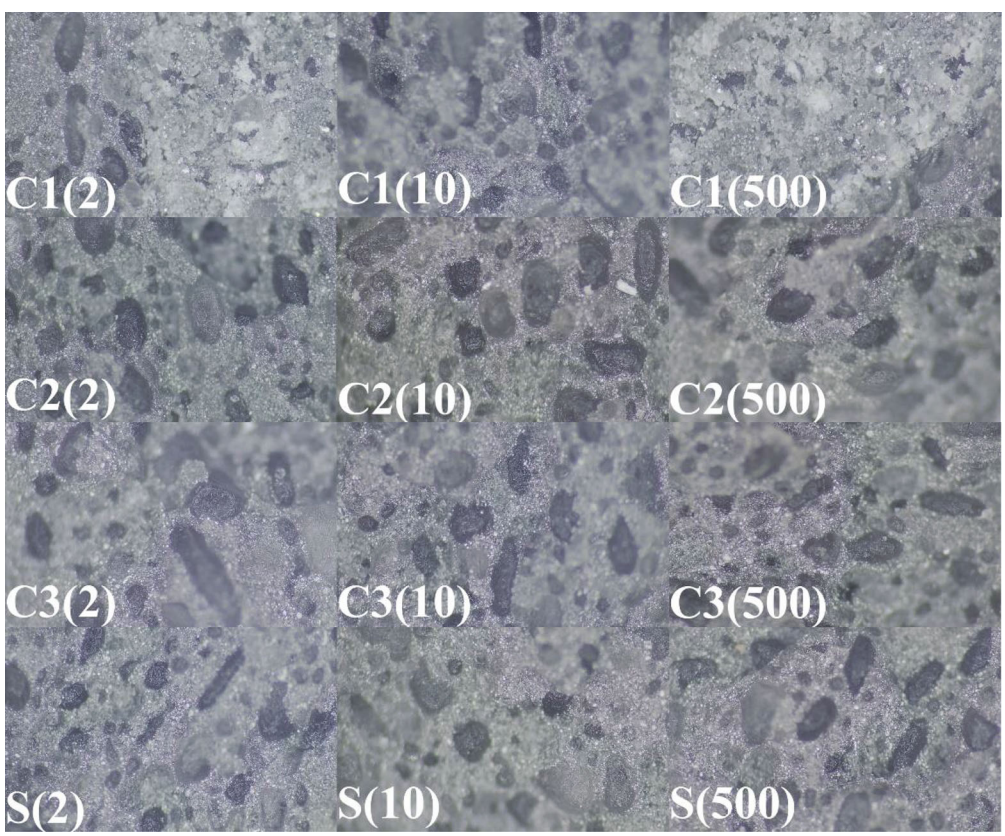

Figure 11: Specimen fracture shape.

cross-sections. Therefore, in this study, dumbbell-type HTPB propellant specimens were uniaxially stretched until they broke, and the fractured specimens were placed before a microscope camera to observe their cross-sections. The internal filling coefficient was high, and the particle clusters were surrounded by HTPB base. Small particles were embedded between large particles, but there were also certain pores and microcracks. Most of the particles were approximately spherical or ellipsoidal, and the surfaces were smooth, essentially complete particles and "pits left by duetting" of the particles, because the observed cross-sections were formed by breaking the HTPB propellant. The "dehumidification" of the HTPB propellant was the primary reason for its failure under uniaxial tensile loading, as is shown in Figure 11.

4. Conclusions

4.1. Under Low (Less Than 10 mm/min) Uniaxial Tensile Rates, Crack Propagation in the Propellant Exhibited Three Distinct Stages: A Linear Stage, a Yield Stage, and a Failure Stage. However, under a high (500 mm/min) uniaxial tensile rate, the crack growth did not have a significant yield stage and went directly from the linear stage to the failure stage, which lasted only for a short time. In the C1, C2, C3, and S groups, the tensile rate significantly affected the ultimate strain, and the ultimate failure strain gradually decreased as the tensile rate changed from 2 mm/min to 10 mm/min, and finally to 500 mm/min. Additionally, the proportion of brittle failure in the fracture increased.

4.2. The Microscopic Topographies of the HTPB Propellant Cross-Sections Were Observed Using the MP Technique, and It Was Found That the Solid Particles in the HTPB Propellant Had a High Filling Coefficient and Were Surrounded by Clusters. The small particles and the large particles were embedded in the matrix, and the particles were mostly spherical or ellipsoidal. The surfaces were smooth, and there were certain pores, microcracks, and other defects.

4.3. The Specimen Fractures Showed That the Closer a Fracture Was to the Edge of the Specimen, the Closer the Fracture Was to a Positive Fracture. Additionally, the shapes of the specimens after fracture corresponding to different crack inclination angles showed that the closer a fracture was to a positive fracture, the straighter was the edge notch of the specimen.

Data Availability

The data supporting the conclusion of the article are shown in the relevant figures and tables which are included within the article.

Conflicts of Interest

The authors declare that there are no conflicts of interest regarding the publication of this article.

Acknowledgments

This work was supported in part by the National Natural Science Foundation of China under grant 11962021 and Inner Mongolia Natural Science Foundation Project (2021MS05020).

References

[1] T. Feng, J. Zheng, J. S. Xu, L. Han, and N. Kang, "Mesoscopic structure modeling and numerical simulation of debonding process of composite solid propellants," *Journal of Aerospace Power*, vol. 33, no. 1, p. 9, 2018.

[2] Z. X. Gu, J. Zheng, W. Peng, and J. Z. Zhi, "A viscoelastic constitutive model of solid composite propellants with microcracking damage," *Acta Materiae Compsoitae Sinica*, vol. 35, no. 5, p. 8, 2018.

[3] J. J. Fan, G. Y. Liu, J. H. Zhang, and H. Zhu, "Effect of loading rate on tensile fracture behavior of silicon rubber," *Materials for Mechanical Engineering*, 2007.

[4] H. Li, S. X. Wang, M. Li, J. S. Xu, X. G. Fan, and X. Chen, "Experimental research on tensile mechanical properties of NEPE propellant under confining pressure," *Propellants, Explosives, Pyrotechnics*, vol. 45, no. 11, pp. 1769–1779, 2020.

[5] Y. X. Liu, S. Q. Hu, Y. J. Zhang, X. J. Fu, L. Ren, and H. Y. Li, "Mechanical properties of modified double-base propellant under different tensile rates," *JOURNAL OF PROPULSION TECHNOLOGY*, vol. 43, no. 1, p. 6, 2022.

[6] X. L. Chang, B. Long, K. Hu, and W. L. Zhao, "Progress of study on the fracture performance," *Chinese Journal of Explosive & Propellants*, vol. 36, no. 3, p. 8, 2013.

[7] G. C. Zhu, S. Yuan, C. Y. Liu et al., "Mechanical properties of quasi-static stretch of HTPE/AP/Al/RDX propellant," *Chinese Journal of Explosive & Propellants*, vol. 44, no. 5, p. 7, 2021.

[8] T. Seyidoglu and M. A. Bohn, "Effects of four isocyanates and four plasticizers on the thermomechanical and tensile properties of hydroxyl-terminated polybutadiene elastomers and the effect of solid particle filling," *Journal of Applied Polymer Science*, 2020.

[9] S. J. Geng, B. Sun, and J. W. Zhang, "Numerical computation of mixed mode crack propagation in solid propellant," *Journal of Solid Rocket Technology*, vol. 34, no. 1, p. 5, 2011.

[10] H. L. Gao, H. Liu, Z. C. Qi, H. Liu, and H. B. Zheng, "Research on variation law of fatigue crack-tip displacement and strain fields based on high-speed digital image correlation method," *ACTA ARMAMENTARII*, vol. 36, no. 9, pp. 1772–1781, 2015.

[11] T. Y. Wang, J. S. Xu, H. Li, D. Wu, J. M. Liu, and X. Chen, "Crack propagation velocity and fracture toughness of hydroxyl-terminated polybutadiene propellants: experiments and simulations," *Engineering Fracture Mechanics*, vol. 257, p. 108034, 2021.

[12] C. M. Jarocki, T. D. Manship, and S. F. Son, *Investigation of Mechanical Properties of AP/Al/HTPB-Based Propellants Using 2-D Digital Image Correlation at Lage and Small Scale*, AIAA, 2021.

[13] M. Hamidpour, M. R. Nami, A. Khosravifard, and M. Lévesque, "Modeling fracture in viscoelastic materials using a modified incremental meshfree RPIM and DIC technique," *European Journal of Mechanics - A/Solids*, 2021.

[14] Q. Xu, Q. Z. Fang, B. L. Sha, and Q. W. Hu, "Study on a damage model of NEPE solid propellant based on a Weibull

distribution," *Mechanics of Time-Dependent Materials*, pp. 1–16, 2021.

[15] H. Cui, "Zhou numerical simulation of crack propagation in solid propellant based on cohesive zone model," *Meccanica*, vol. 24, no. 1, pp. 63–68, 2012.

[16] X. W. Li, Z. S. Yao, X. H. Liu, and X. W. Huang, "Energy evolution and damage mechanism of fractured sandstone with different angles," *Energies*, 2022.

[17] C. Le, X. Ren, H. Wang, and S. Yu, "Experimental and Numerical Study on the Failure Characteristics of Brittle Solids with a Circular Hole and Internal Cracks," *Materials*, vol. 15, no. 4, p. 1406, 2022.

[18] C. T. Liu and C. W. Smith, "Investigating Near Tip Damage Mechanics and Crack Growth Behavior in a Particulate Composite Material," in *In Proceedigs of the Sixth Japan-US Conference on Composite Materials*, pp. 379–387, CRC Press, 2022.

[19] B. Long, S. S. Gao, and W. Jin, "Study on the crack-tip fields of solid propellant grains at the ignition transient," *Journal of Projectiles, Rockets, Missiles and Guidance*, 2021.

[20] F. Gao and Z. Zhang, "Review on performance evaluation of solid rocket motors with charge defects," *ACTA ARMAMENTARII*, 2021.

[21] Y. Wang, G. C. Li, X. Zhang, Y. H. Han, and X. Li, "Analysis of crack tip propagation process of HTPB propellants based on SEM and digital correlation method," *Chinese Journal of Explosives & Propellants.*, 2019.

[22] Q. Q. Yang, S. L. Xu, R. L. Cai, J. Zhang, F. Z. Qiang, and Z. P. Huang, "Mesoscopic damage behavior of composite solid propellants based on digital image processing technology," *Journal of Solid Technology*, 2022.

[23] Y. Wang, G. C. Gao, P. Wu, M. Yang, and Y. H. Han, "J-integral measurement of mixed mode cracks of HTPB propellants based on digital correlation method," *ACTA ARMAMENTARII*, 2019.

[24] Aerospace Industry Standards of the Ministry of Aerospace Industry of the People's Republic of China, "QJ924-85, Test method for uniaxial tension of composite solid propellant," 1985.